Research Article

Ramana G. Reddy*

High-temperature production of AlN in Mg alloys with ammonia gas

https://doi.org/10.1515/htmp-2022-0307 received June 17, 2023; accepted December 17, 2023

Abstract: The objective of this study was to produce composites with a uniform distribution of aluminum nitride (AlN) reinforcing particles in the magnesium (Mg) metal matrix composites. In this study, experiments were carried out to evaluate the effect of time and temperature on the nitridation of aluminum to form AlN and its distribution in Mg composites. High-temperature production of AlN in Mg alloys melts using the ammonia gas bubbling method was investigated. The effect of ammonia bubbling time and temperature at a flow rate of 0.1 liters per minute on the amount of AlN formation was studied. Bubbling of ammonia gas resulted in the in-situ formation of AlN in Mg alloys, yielding AlN-reinforced Mg alloy composites. The AlN formation in the alloy was increased with increasing bubbling time. The rate of AlN formation was found to be 0.34 g·min⁻¹ at 1,073 K. An average yield of AlN (wt%) was 6.47, 29.65, and 27.43 at 973, 1,073, and 1,173 K, respectively. An activation energy of 59.57 kJ was determined for the nitridation process. The magnitude of activation energy indicates that the reaction proceeds in the mixed regime with control of both nucleation and interface diffusion. The product was characterized using X-ray diffraction (XRD), optical microscopy, and scanning electron microscopy. The characterization of samples showed that the AlN particles distributed throughout the alloy matrix. The AlN particles formed in-situ are small in size, and uniform dispersion of AlN particles was observed at higher bubbling times and at higher temperatures. The AlN crystallite size increased with an increase in bubbling time and temperature. The XRD characterization results showed that the composite formed in-situ was composed of (Mg), intermetallic y-(Mg, Al), and AlN phases. The Rockwell hardness of the in-situ composites was higher than the unreinforced Mg alloy, and the hardness increased with an increase in the AlN wt% in the Mg alloy composites.

Keywords: magnesium alloys, aluminum nitride, ammonia gas, nitridation reaction rate

1 Introduction

A metal matrix composite (MMC) comprises a metallic base with a reinforcing constituent, which is usually non-metallic and is commonly ceramic. Discontinuously reinforced aluminum alloy composites are a class of MMCs that have tremendous potential for structural applications. Reinforcing the matrix with the hard ceramic phases improves the wear resistance, tensile strength, and elastic modulus of the metallic materials. Aluminum and magnesium alloy composites reinforced discontinuously with ceramic particles are of special interest to the automotive, defense, military, and aerospace applications owing to their excellent properties such as low density, high specific strength, high specific stiffness, and lower cost. Magnesium has a lower density (about 1.74 g·cm⁻³), which makes its composites lighter in weight.

The magnesium (Mg) MMCs can be obtained by various techniques [1,2], such as via liquid, solid, and vapor state processing. A simplified processing flow sheet for MMCs is shown in Figure 1. The liquid state processing is extensively investigated, and it includes several processes such as stir casting, squeeze infiltration, spray deposition, semisolid casting, pressure infiltration, in-situ reaction synthesis, and pressure-less infiltration. The process path used in this investigation for the in-situ reaction synthesis of aluminum nitride (AlN)-reinforced Mg alloy MMCs is highlighted in red in Figure 1. Magnesium alloys and their properties are discussed in previous studies [3-9]. SiC-reinforced Mg alloy composites synthesized using the above production routes have been extensively studied [10-16]. Although magnesium MMCs obtained from these conventional techniques have demonstrated a strong position for weight-critical applications, they are still not profitable for structural applications. Magnesium matrix composites using different combinations of reinforcements and their effects on the chemical, mechanical, and tribological properties were discussed [17–28].

^{*} Corresponding author: Ramana G. Reddy, Department of Metallurgical and Materials Engineering, The University of Alabama, Tuscaloosa, AL 35487, USA, e-mail: rreddy@eng.ua.edu

2 — Ramana G. Reddy DE GRUYTER

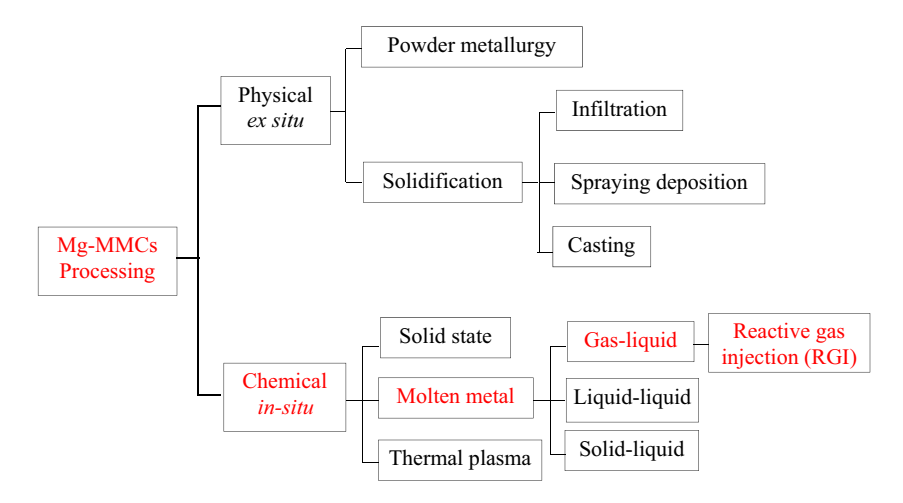


Figure 1: Processing of Mg-MMCs [1,2].

In solidification, the reinforcement is introduced into molten metal using conventional foundry melting processes, while in the powder metallurgy approach, the matrix metal and reinforcement powder are mixed, consolidated, and fired to form the composites. Squeeze casting is a popular MMC fabrication route, especially for adding randomly aligned short alumina fibers such as Saffil. Short fiber reinforcements increase elastic modulus, proof stress, and tensile strength dependent on volume fraction while severely restricting elongation to failure. Stir casting is typically employed for the fabrication of particulate-reinforced composites. An increase in the strength of many magnesium alloys prepared by powder metallurgy as opposed to ingot metallurgy indicates that composite materials derived using PM techniques may show improved properties. The improvement in properties such as proof stress, tensile strength, and elastic modulus for several magnesium alloys was observed.

Particle-reinforced magnesium matrix composites are produced by squeeze casting [29], stir casting [11–14], powder metallurgy [15], and spray forming [16]. These methods involve the incorporation of reinforcing second-phase particles, which include borides, carbides, and nitrides, into molten magnesium by ex situ methods. The drawbacks are that the reinforcing particle size is coarse, and also interfacial reaction and poor wettability between the reinforcements and the matrices due to surface contamination of the reinforcements.

The *in-situ* processing, in which the reinforcing particles are directly formed from *in-situ* chemical reactions, is quite promising for MMC manufacturing [30]. This process involves a gas—liquid reaction that leads to reinforcement formation [31,32]. The reinforcing particles are formed when the bubbling gas reacts with the matrix melt. SiCreinforced Mg alloy MMCs can be obtained by bubbling

carbon-bearing gases through the Mg–Si melt. AlN-reinforced Mg alloy MMCs can be obtained by bubbling nitrogen-bearing gases through the Mg–Al melt. Using this technology, aluminum alloy composites reinforced with TiC [33], SiC [34,35], and AlN [36–38] and magnesium alloy composites reinforced with AlN [39] have been successfully processed. The advantage of this method is that the forced agitation due to the bubbling gas improves the uniformity of reinforcement dispersion; also, the availability of a large gas–liquid contact area provides fast reaction kinetics. It is estimated that this *in-situ* production process cost is about 1/3 less than the conventional process.

This article presents the experimental results of high-temperature *in-situ* synthesis of AlN in Mg alloys melts using ammonia gas. The effect of ammonia bubbling time and temperature on the yield of AlN-reinforced Mg alloy composites was studied. Microstructural characterization of samples using X-ray diffraction (XRD), optical microscopy (OM), and scanning electron microscopy (SEM) results is presented. The reaction rates and activation energy of the nitridation process and AlN distribution in Mg alloy matrix results are discussed.

2 Experimental

The experimental setup for *in-situ* processing of Mg composites is shown in Figure 2. The Lindberg® furnace consists of a working chamber, heating elements, an insulator, a standard type-S (Pt–10% Ru/Pt) thermocouple, and a control console. In the furnace, an overall 14 cm constant temperature zone with a variation of ± 5 K can be obtained. The *in-situ* reaction was performed in an alumina crucible

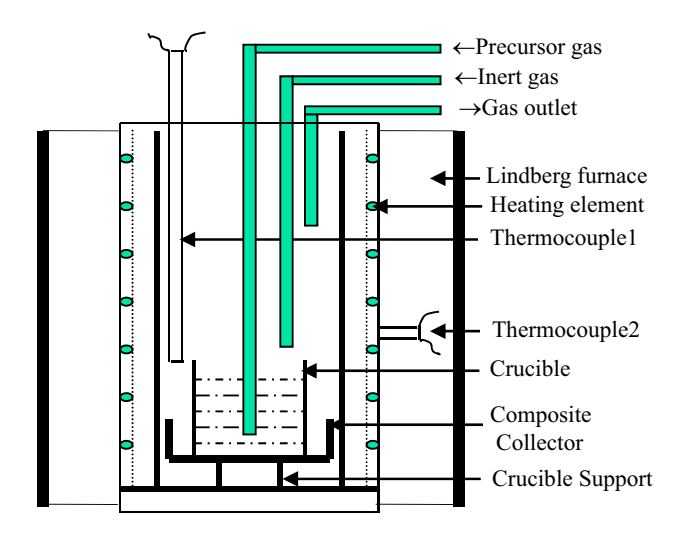


Figure 2: Schematic diagram of experimental setup.

located in the uniform temperature zone of the furnace tube. The dimensions of the alumina crucible are 2.5 cm in diameter and 5 cm in height. The gas bubbling tube is an alumina tube with a nozzle diameter of 1.5 mm, which was immersed into the melt near the bottom of the reactor in the bubbling process. The bottom end of the furnace is closed, and the upper end is sealed by a furnace cover. The furnace tube was purged with pure argon (99.999% purity) throughout the experiments.

The alloy composition studied was 30% Al and balance Mg. Pure Mg rods (99.9% purity, purchased from Good Fellow Corp.®) and Al granules (99.99% purity, purchased from Alfa Aesar®) were used to make the desired alloy. Ammonia gas was of 99.999% purity. Mg and Al were mixed in the alumina crucible with a capacity of 100 ml to obtain the required composition of the alloy, and the crucible was then placed in the furnace tube in the constant temperature zone. The Mg-Al mixture was used to better control the distribution of AlN particles formed in the melt. The furnace tube was sealed with a furnace cover after loading the reaction crucible and setting the thermocouples and gas-delivering tubes in suitable positions. All experiments were conducted with an ammonia gas flow rate of 0.1 LPM (liters per minute). The alloy components were mixed thoroughly prior to heating in the furnace. On reaching the predetermined temperature, the alloy was allowed to homogenize at a constant temperature for about 15 min. The bubbling tube was then submerged into the melt up to the bottom of the crucible, and bubbling gas (NH $_3$) was introduced into the melt. The residual NH $_3$ was scrubbed before the NH $_3$ -free gas was vented using an ammonia scrubber (which uses dilute sulfuric acid to neutralize the ammonia). The entire process was monitored through the eyehole on the furnace cover. NH $_3$ gas was bubbled into the melt for different time periods, and its effect on product composition was studied. After the bubbling period, the furnace was turned off, and the products were allowed to cool and solidify in the furnace under an argon atmosphere.

The reaction products were analyzed using various characterization techniques. Phases in the product were characterized using a powder XRD technique (Philips-Electronic APD 3600 modified X-ray diffractometer). The microstructure of the composite was studied using OM. The compositional analysis of the final product was performed using energy-dispersive spectrometry (EDS).

3 Results and discussion

3.1 Effect of bubbling time on product morphology and formation of AlN at 1.173 K

The effect of NH_3 gas bubbling time on AlN yield at a constant flow rate of 0.1 LPM and a temperature of 1,173 K was studied, and the results are shown in Table 1. AlN was formed *in-situ* in the magnesium alloy according to the reaction shown in equation (1) [40,41]

$$2 \text{Al}_{(1)} + 2 \text{NH}_{3(g)} = 2 \text{AlN}_{(s)} + 3 \text{H}_{2(g)}. \tag{1}$$

$$\Delta G_{(1)}^o = -548,116 + 1.0593 T \text{ J}.$$

$$Mg_3 \text{N}_{2(s)} + 2 \text{Al}_{(1)} = 3 \text{Mg}_{(1)} + 2 \text{AlN}_{(s)}. \tag{2}$$

$$\Delta G_{(2)}^o = -169,123 - 0.41 T \text{ J}.$$

Table 1: Effect of time on AIN formation (experimental conditions: 1,173 K, 0.1 LPM)

Experiment number	Starting weight of alloy (g)	Bubbling time (min)	Weight of AIN formation (g)	AIN (wt%)
1	80.59	15	5.09	6.40
2	80.58	45	11.35	14.80
3	80.32	70	21.78	27.43

At 1,173 K, the standard Gibbs energy of the reaction (1) is negative, indicating that AlN is favorable to be formed by bubbling ammonia gas. The thermodynamic analysis shows that Mg_3N_2 formed in the Mg–Al melt is not stable and could be reduced by Al via the reaction given by reaction (2).

The percentage yield of AlN in the Mg alloy was calculated from XRD data [42] and EDS data, and the results are shown in Figures 3 and 4. Figure 3 shows the AlN yield in wt% in the alloy, and Figure 4 shows the AlN yield in grams. It can be seen from Figures 3 and 4 that as the bubbling time is increased, the AlN yield increases, and at 70 min of ammonia bubbling, an average of 27.43 wt% AlN was formed in the Mg alloy.

Figures 5-7 show the optical micrographs and XRD patterns of the alloy product formed after 15, 45, and 70 min of ammonia bubbling at 1,173 K, respectively. It can be seen from the XRD patterns that the product is composed of (Mg), inter-metallic y-(Mg, Al), and AlN. The (Mg) is solid magnesium solution with aluminum dissolved in it, and inter-metallic γ -(Mg, Al) is the gamma phase of stoichiometry Mg₁₇Al₁₂. It can be seen from Figures 5b, 6b, 7b that the primary XRD peak for AlN increased with an increase in bubbling time, indicating that the AlN amount increased in Mg alloy composites, as shown in Figures 3 and 4. Figure 5a and b shows the optical micrograph and XRD of the product formed at an ammonia gas bubbling time of 15 min, respectively. The AlN formed in the alloy was approximately 6.4 wt%. Figure 6a and b shows an optical micrograph and XRD of the product formed after 45 min of ammonia bubbling, respectively. The average AlN formed in the alloy was approximately 14.8 wt%. Figure 7a and b represents the optical micrograph and XRD of the product formed after 70 min of bubbling, respectively, in which the average AlN formed was 27.43 wt%. The average AlN weight formed in the

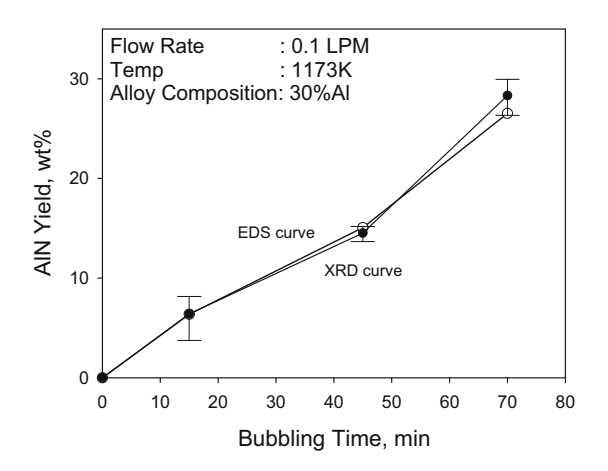


Figure 3: Effect of bubbling time on percentage AIN yield at 1,173 K.

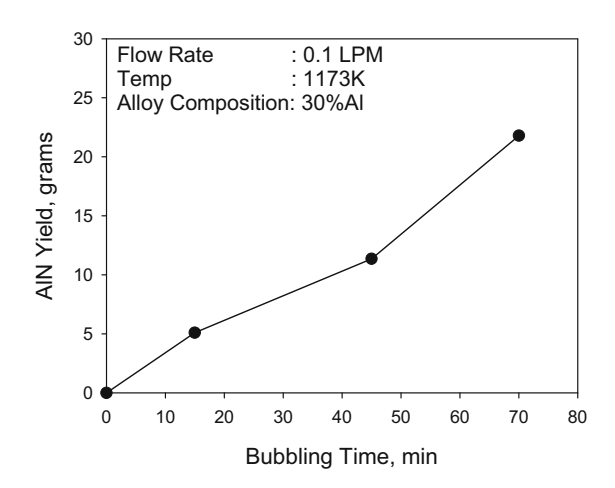
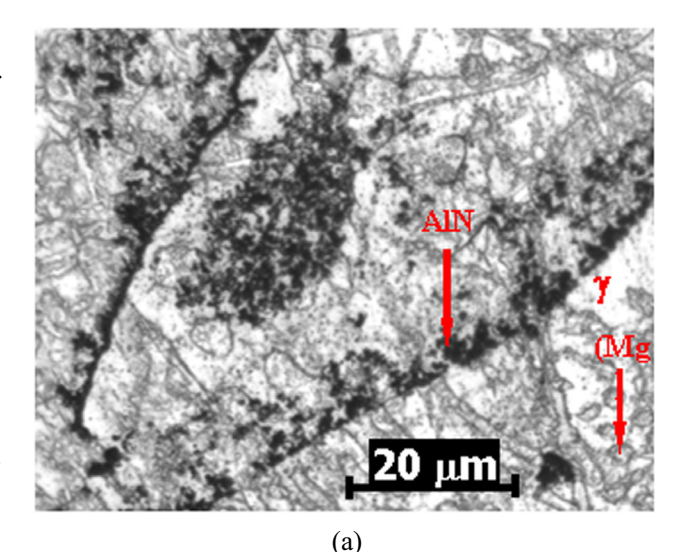


Figure 4: Effect of bubbling time on weight of AIN yield at 1,173 K.



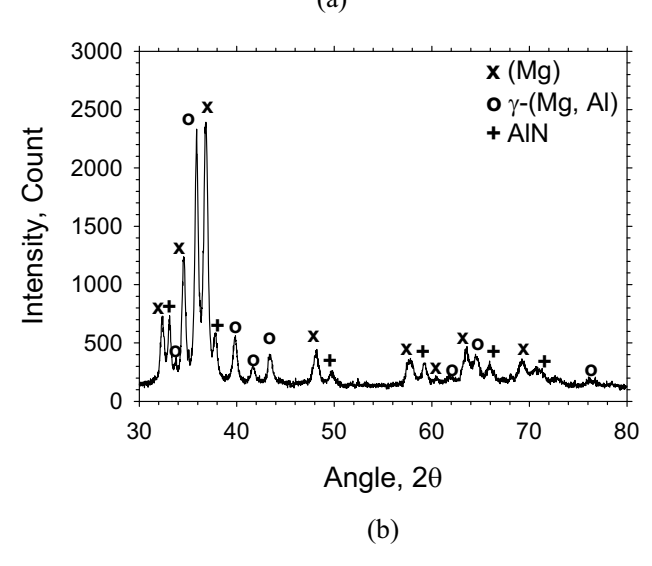


Figure 5: Optical micrograph (a) and XRD pattern (b) of Mg alloy/AIN composites (experimental conditions: 15 min, 1,173 K, 0.1 LPM).

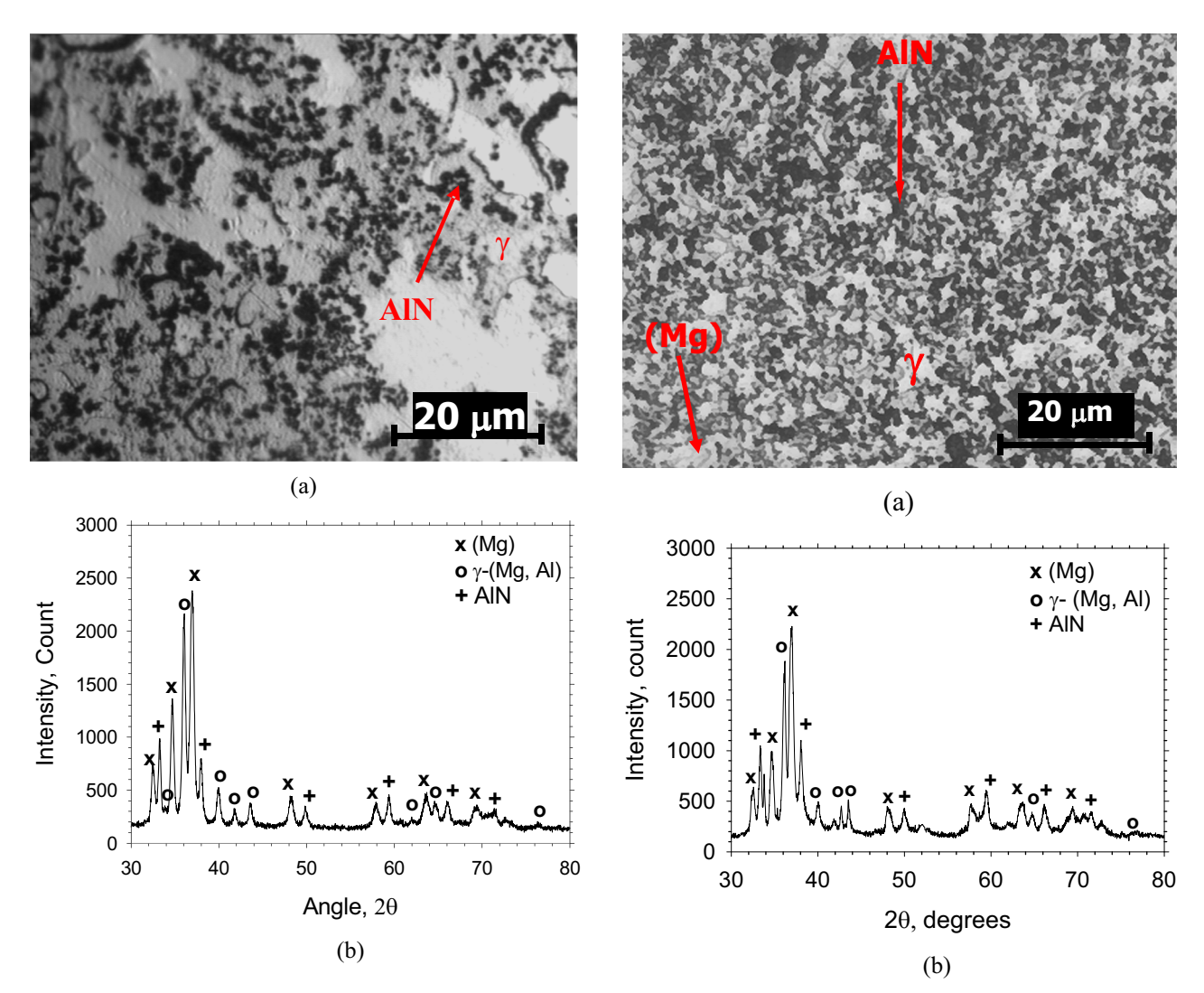


Figure 6: Optical micrograph (a) and XRD pattern (b) of Mg alloy/AlN composites (experimental conditions: 45 min, 1,173 K, 0.1 LPM).

Figure 7: Optical micrograph (a) and XRD pattern (b) of Mg alloy/AlN composites (experimental conditions: 70 min, 1,173 K, 0.1 LPM).

composite was 5.09, 11.35, and 21.78 g for the corresponding bubbling time of 15, 45, and 70 min, respectively. In all the optical micrographs, the gray matrix is the (Mg) phase, the white is γ -(Mg, Al), and the black particles are the AlN particles that are distributed throughout the alloy.

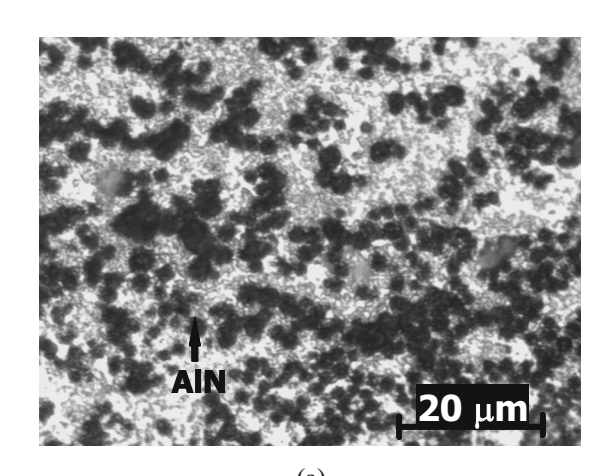
From Figures 5–7, the average AlN crystallite size was calculated from the XRD patterns [42]. The average AlN crystallite size was 1.30 nm at 15 min, 2.03 nm at 45 min, and 3.40 nm at 70 min of ammonia bubbling time. The size of the AlN crystallite size increases with an increase in bubbling time. However, as shown in the micrograph, agglomeration of AlN particles was observed at lower bubbling times.

As shown in Figure 5a, AlN particles are engulfed in the freezing interface. This type of phenomenon is termed a particle–solidification front interaction, where a freely suspended second-phase particle can be either pushed or

engulfed by a freezing interface [43]. Thus, the reinforcing phase generally tends to segregate in the interdendritic liquid instead of being homogenously distributed within cells and dendrites. These interactions are important in determining the final microscopic distribution of reinforcing particles in cast-MMCs. A similar, particle-solidification front interaction phenomenon was observed in this research. From the optical micrograph (Figure 5a), it becomes apparent that the AlN particles segregate to interdendritic regions at lower bubbling times. In Mg alloy/AlN composites, it is observed that each AlN particle appears to be surrounded by γ-(Mg, Al) intermetallic. A similar microscopic distribution of reinforcing particles was observed [44]. They observed that each SiC ceramic particle is surrounded by γ-(Mg, Al) intermetallic. Thus, it is encountered in this research that during the solidification of composite products, the AlN particles are pushed by the growing magnesium-rich dendrites into the last

5 — Ramana G. Reddy DE GRUYTER

solidifying interdendritic regions. As the bubbling time increases, the AlN yield increases thus, the particles get uniformly dispersed, and also their dispersion density increases. Due to the lower yield of AlN at a bubbling time of 15 min, Figure 5a shows a lower dispersion density of AlN particles than that at 45 and 70 min, as shown in Figures 6a and 7a, respectively. The dispersion of AlN particles is uniform, as shown in Figure 7a, for a bubbling time of 70 min. Thus, an increase in AlN yield is observed when the bubbling time increases at a flow rate of 0.1 LPM (Figures 3 and 4). The solubility of hydrogen in Mg is very low (2.36 \times 10⁻⁴ wt% H at 1,173 K). The forced agitation due to bubbling gas improves the uniformity of reinforcement dispersion and because of no hydrogen reaction with alloy, hydrogen gas was removed from the melt and resulted in no porosity in the Mg alloy composites.



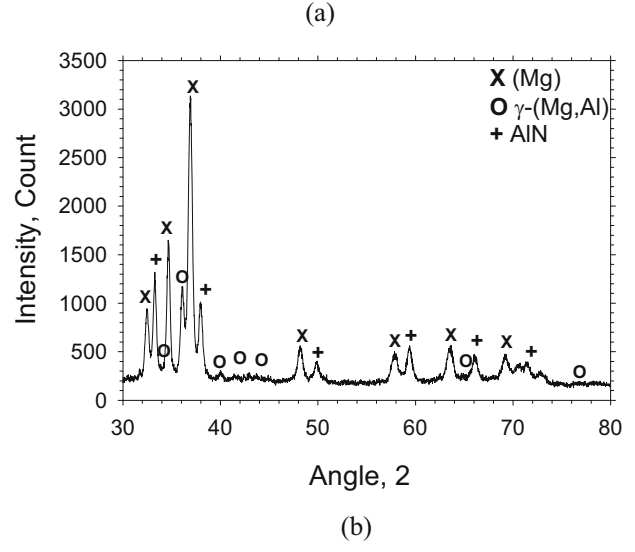


Figure 8: Optical micrograph (a) and XRD pattern (b) of Mg alloy/AIN composites (experimental conditions: 1,073 K, 70 min, 0.1 LPM).

3.2 Effect of temperature on product morphology and formation of AIN at 1,073 K

Experiments were conducted by bubbling ammonia gas for 70 min through the melt at 1,073 K and a flow rate of 0.1 LPM. Figure 8a and b shows the optical micrograph and XRD pattern of the AlN in Mg-alloy composites. When ammonia bubbled through the Mg alloy melt, a significant amount of AlN was formed throughout the alloy. The composite product weight was increased due to the formation of AlN. The phases were identified to be Mg solid solution (aluminum dissolved in it), gamma phase γ -(Mg, Al), and AlN. The sample analyses showed that the average percentage of AlN is about 29.65 wt% or an average weight of 23.62 g in the composite. From the OM micrograph, it can be seen that AlN particles are dispersed uniformly throughout the product and are surrounded by Mg solid solution.

3.3 Effect of temperature on product morphology and formation of AIN at 973 K

Figure 9 shows the SEM micrograph of the composites formed *in-situ* by bubbling ammonia gas for 70 min through the melt at 973 K and a flow rate of 0.1 LPM. Table 2 lists the EDS analysis of several area scans marked in Figure 9. EDS analysis confirms that area A is (Mg), area B is y-(Mg, Al),

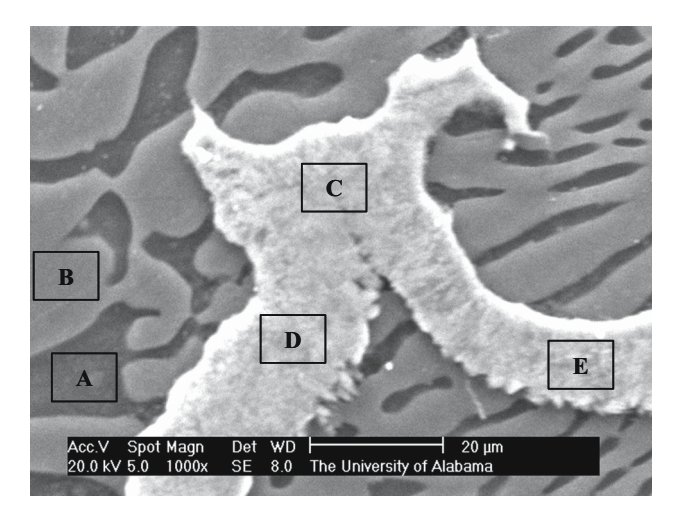


Figure 9: SEM micrograph of Mg alloy/AIN composites. (experimental conditions: 973 K, 70 min, 0.1 LPM).

DE GRUYTER Mg-AIN alloy composites — 7

Table 2: EDS analysis of areas shown in Figure 9 for composites formed *in-situ* by bubbling ammonia gas for 973 K, 70 min, and flow rate of 0.1 LPM

Area	Composition in At%	Phase	
A	Mg = 89.41	(Mg)	
	AI = 10.59		
В	Mg = 64.96	γ-(Mg, Al)	
	AI = 35.04		
C	N = 29.75	AIN-rich region	
	Mg = 17.10		
	AI = 53.14		
D	N = 28.43	AlN-rich region	
	Mg = 17.41		
	AI = 54.16		
Е	N = 27.89	AlN-rich region	
	Mg = 16.89		
	AI = 55.22		

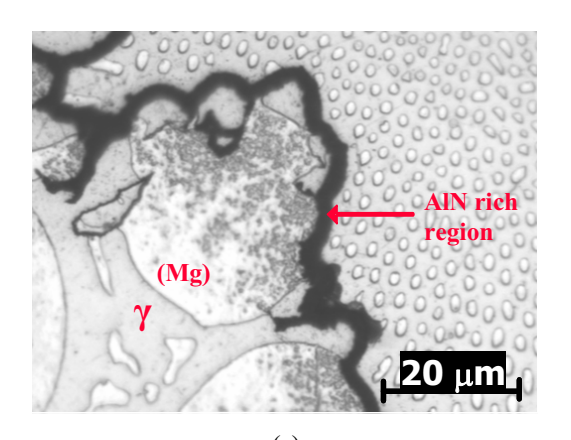
whereas areas C, D, and E show a high percentage of Al and N with a small amount of Mg in them. As N cannot be present in the elemental form in the melt, it reacts with Al and forms AlN. Thus, the areas shown in C, D, and E are AlN, which are covered with Mg alloy. A large amount of γ -(Mg, Al) phase is seen in the SEM micrograph because a smaller amount of Al has reacted with N to form AlN. At a reaction temperature of 973 K, it is not possible to form distinct AlN particles. Instead, AlN-rich regions in the form of dense layers were seen to be formed throughout the melt.

Figure 10a and b shows the optical micrograph and XRD pattern of the sample composites formed *in-situ* by bubbling ammonia gas for 70 min through the melt at 973 K at a flow rate of 0.1 LPM. The XRD results show that at this low temperature, AlN was formed, but the yield was less (6.47 wt% or an average weight of 6.45 g). Figure 10a shows the optical micrograph of the composites. The formation of a dense layer of AlN in the Mg alloy agrees with the work reported [45]. They reported that three forms of AlN can be formed *in-situ*, such as dense layer, dispersed particles, and pure AlN ceramics, depending on processing parameters.

The average AlN crystallite size was calculated from the XRD data given in Figures 7 and 8 [42]. The average AlN crystallite size was 2.88 nm at 1,073 K and 3.40 nm at 1,173 K for an ammonia bubbling time of 70 min and 0.1 LMP. Because of a dense layer formation at a reaction temperature of 973 K, it was not possible to form isolated AlN particles. It can be seen from Figures 7b and 8b that the primary XRD peak for AlN increased with an increase in temperature. The AlN crystallites increases with an increase in temperature.

3.4 Effect of temperature on AlN yield in Mg alloy/AlN composites

Figure 11 shows the percentage of AlN yield in the composite, while Figure 12 shows the AlN yield in grams as a function of temperature at a bubbling time of 70 min and a gas flow rate of 0.1 LPM. Flow rate, bubbling time, and alloy composition were kept constant in these experiments,. The representative error bars in Figure 12 are in the same range as shown in Figure 11. At 973 K, the yield was lower due to the incomplete melting of the alloy and slower reaction kinetics. As shown in Table 3, at 973 K, the average yield of AlN in weight percentages was found to be 6.47%, 29.65% at 1,073 K, and at 1,173 K, it was about 27.43%. The average weight of AlN in grams was found to be 6.45, 23.62, and 21.78 g at 973, 1,073, and 1,173 K, respectively.



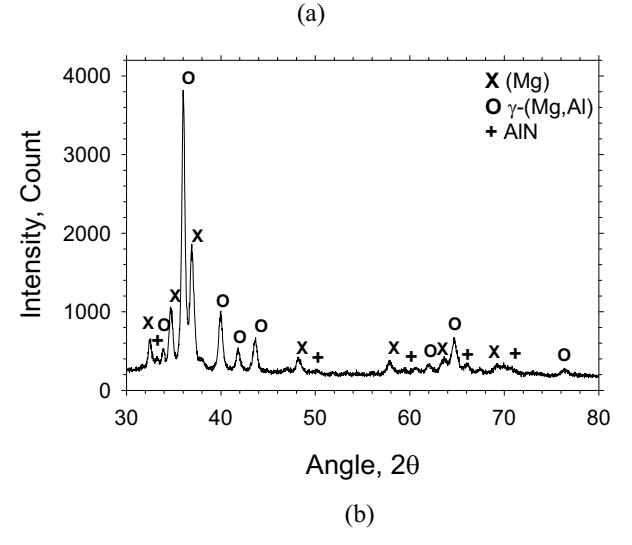


Figure 10: Optical micrograph (a) and XRD pattern (b) of Mg alloy/AlN composites (experimental conditions: 973 K, 70 min, 0.1 LPM).

8 — Ramana G. Reddy DE GRUYTER

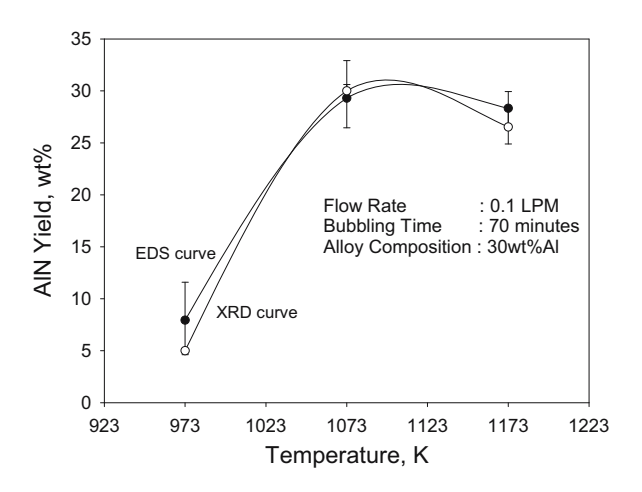


Figure 11: Effect of temperature on the percentage AlN yield in Mg alloy/ AlN composites (experimental conditions: 70 min, 0.1 LPM).

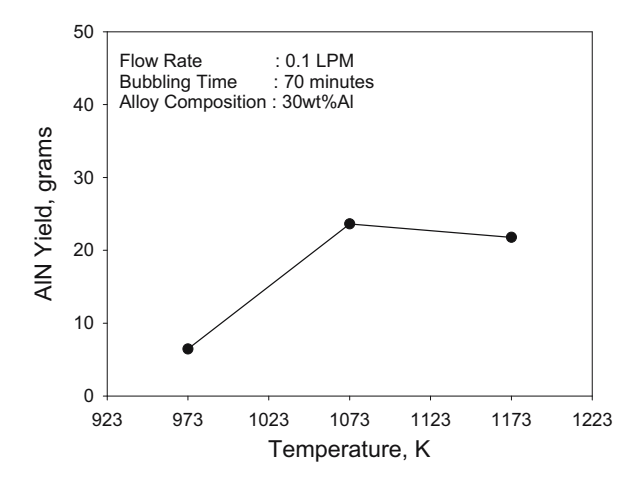


Figure 12: Effect of temperature on the weight of AlN yield in Mg alloy/ AlN composites (experimental conditions: 70 min, 0.1 LPM).

3.5 Rate of AlN formation (R_{AIN}) in Mg-Al alloy/AlN composites

The rate of formation AlN ($R_{\rm AlN}$) in Mg alloy/AlN composites for a bubbling time of 70 min and a gas flow rate of 0.1 LPM was calculated as a function of temperature. Table 3 shows the calculated results. The overall rate of AlN formation, $R_{\rm AlN}$, is found to be 0.34 g·min⁻¹ at 1,073 K in the Mg alloy. This is slightly higher than that reported for the *insitu* formation of AlN in the aluminum alloy (Al–5wt% Si) composites, which was 0.23 g·min⁻¹ [38]. In our previous study, it was concluded that diffusion of nitrogen atoms in the liquid boundary layer is assumed to be the rate-controlling step for forming AlN in the Al alloy melts using ammonia as the gaseous precursor [38]. The increase in the rate of formation of AlN in this study may be due to the catalytic effect of Mg promoting the nitridation of Al to AlN.

Table 3: Rate of AlN formation (R_{AlN}) as a function of temperature of Mg alloy/AlN composites (experimental conditions: 70 min, 0.1 LPM)

Exp no.	<i>T</i> (K)	AIN (wt%)	Weight of AIN formed (g)	R _{AIN} (g·min ^{−1})
1	973	6.47	6.45	0.09
2	1,073	29.65	23.62	0.34
3	1,173	27.43	21.78	0.31

The activation energy of reaction (E_a) was determined using the Arrhenius relationship shown in equation (3):

$$R_{\rm AlN} = Ae^{\frac{-E_a}{\rm RT}},\tag{3}$$

where $R_{\rm AlN}$ is the rate of AlN formation, A is a rate constant, $E_{\rm a}$ is the activation energy, R is the gas constant, and T is the temperature. From equation (3), we obtain

$$\ln R_{\text{AlN}} = \ln A - \frac{E_a}{RT}.$$
 (4)

The experiments conducted at 973, 1,073, and 1,173 K were used to determine the activation energy. The $\ln R_{\rm AlN}$ vs 1/T plot is presented in Figure 13. The representative error bars in Figure 13 are in the same range as shown in Figures 3 and 11. It was found that

$$\ln(R_{\rm AlN}) = 5.1701 - \frac{7165.2}{T},\tag{5}$$

and $E_{\rm a}$ was calculated to be 59.57 kJ. This is higher than the reported activation energy of 28.72 kJ for the *in-situ* formation of AlN in the aluminum alloy (Al–5 wt% Si) composites bubbling with ammonia gas [38]. They concluded that the rate-controlling step for the formation of AlN from

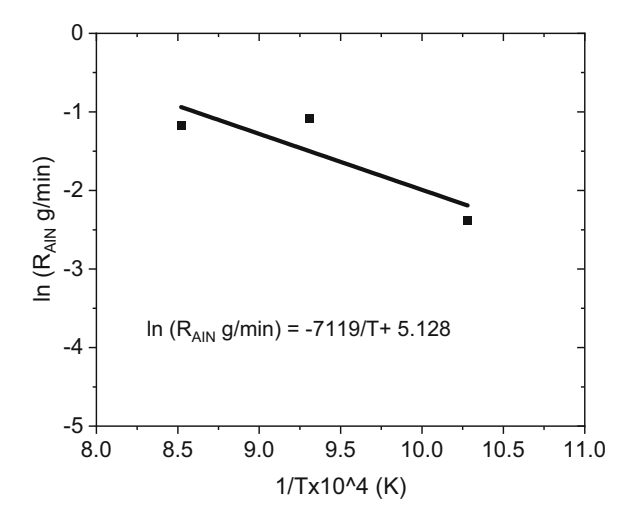


Figure 13: Effect of temperature on the rate of AlN formation in Mg alloy/AlN composites (experimental conditions: 70 min, 0.1 LPM).

DE GRUYTER Mg-AIN alloy composites — 9

bubbling ammonia is the diffusion of nitrogen atoms in the liquid boundary layer. For the in-situ formation of Al-Si-SiC composite bubbling with CH₄ gas [46], it was found that the activation energy was 92 kJ for the temperature range of 1,373-1,573 K, and they concluded that it is a mixed regime where both control the rate of the reaction: nucleation at the interface and diffusion. In the present study, the Mg-Al-AlN composite bubbling with ammonia gas, the magnitude of activation energy indicates that the reaction proceeds in the mixed regime with control of both nucleation at the interface and diffusion. As discussed above (Figures 5, 9 and 10), the particle-solidification front was observed. From these, it becomes apparent that the AlN particles segregate to interdendritic regions at lower bubbling times and also at lower temperatures. The AlN particle appears to be surrounded by y-(Mg, Al) intermetallic phase. Further studies are needed to fully understand the AlN particle interactions with the y-(Mg, Al) intermetallic phase.

3.6 Effect of AlN formation on the hardness of the Mg alloy composites

The Rockwell hardness of the bulk Mg alloy/AlN composites was measured. The Rockwell hardness testing was conducted by using the "N" Brale indenter with a load of 30 kgf. The hardness value, HR30N, was directly read from the Rockwell scale. Figure 14 shows the plot of HR30N values vs AlN wt%. Each hardness measurements were made 3–5 repetitions, and average values and deviation

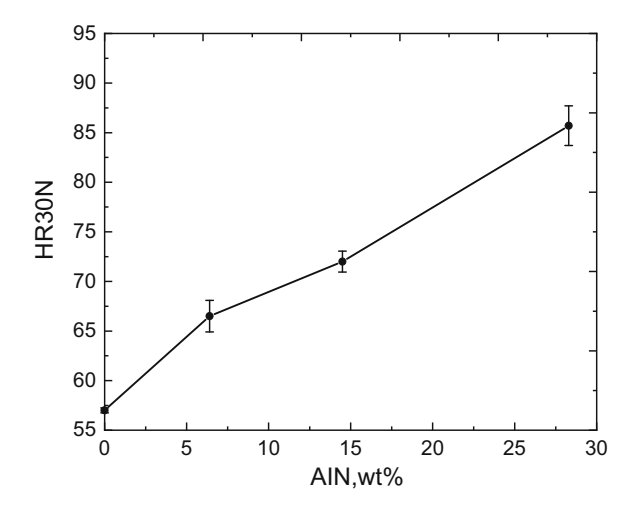


Figure 14: Rockwell hardness values as a function of AIN wt% in Mg alloy/AIN composites (experimental conditions: 1,173 K, 0.1 LPM).

are shown in Figure 14. The HR30N value at 0 wt% of AlN is for Mg alloy without ammonia gas bubbling. The HR30N values at 6.4, 14.8, and 27.43 wt% of AlN formation in Mg alloy/AlN composites with 15-, 45-, and 70-min bubbling time at 1,173 K and a gas flow rate of 0.1 LPM. It can be seen from Figure 14 that the hardness values of *in-situ* composites were higher than the un-reinforced Mg alloy, and the hardness values increased with an increase in the AlN wt% in the Mg alloy composites.

4 Conclusions

The AlN-reinforced Mg MMCs are feasible to form using the in-situ gas bubbling method. Using ammonia led to the formation of AlN in the entire melt at the 0.1 LPM of the ammonia gas flow rate with a bubbling time of up to 70 min and temperatures from 973 to 1,173 K. The AlN formation in the composite increased with increasing bubbling time. The average AlN weight percentage formed in the composite was 6.4, 14.8, and 27.43% for the corresponding bubbling time of 15, 45, and 70 min, respectively. The rate of AlN formation was found to be 0.34 g·min⁻¹ at 1,073 K. The optical micrograph analysis showed the gray matrix of the (Mg) phase, the white phase of y-(Mg, Al), and the black AlN particles which are distributed throughout the alloy. The XRD results showed that the composite formed in-situ was composed of (Mg), intermetallic γ-(Mg, Al), and AlN phases. The size of the AlN crystallites increases with an increase in bubbling time. An average AlN crystallite size calculated from XRD patterns was 1.30 nm at 15 min, 2.03 nm at 45 min, and 3.40 nm at 70 min of ammonia bubbling time. Uniform dispersion of AlN particles was observed at higher bubbling time, while at lower bubbling time agglomeration of AlN particles was observed.

The effect of temperature on AlN formation was studied. The average yield of AlN (wt%) was 6.47, 29.65, and 27.43 at 973, 1,073, and 1,173 K, respectively. An activation energy of 59.57 kJ was determined for the nitridation process. The magnitude of activation energy indicates that the reaction proceeds in the mixed regime with control of both nucleation at the interface and diffusion. The particle-solidification front was observed at low temperature and lower bubbling time, and the AlN particle appears to be surrounded by the γ -(Mg, Al) intermetallic phase. The Rockwell hardness values of *in-situ* Mg alloy composites were higher than the un-reinforced Mg alloy, and the hardness values increased with an increase in the AlN wt% in the Mg alloy composites.

Funding information: The author is pleased to acknowledge the financial support for this research by the National Science Foundation and ACIPCO. The author is pleased to thank the Department of Metallurgical and Materials Engineering (MTE) and the University of Alabama for providing experimental and analytical facilities.

Author contributions: Ramana G. Reddy: conceptualization, methodology, formal analysis, writing – review, editing, and submission.

Conflict of interest: The author states that there is no conflict of interest.

Data availability statement: The experimental raw and processed data needed to reproduce these findings cannot be shared at this time as the data also form part of an ongoing study.

References

- Reddy, R. G. "Aluminum nitride reinforced magnesium alloy composites," IMAT 2023, Detroit, MI, USA, October 2023.
- [2] Clyne, T. W. Metal matrix composites: matrices and processing. Encyclopedia of Materials Science and Technology, A. Mortensen editor., Elsevier, New York, 2001.
- [3] Arya, S. M. and W. D. Griffiths. Metall Mater Trans B, Open Access, Published 22 May 2023.
- [4] Anbuchezhiyan, G., N. M. Mubarak, and R. R. Karri. Mohammad Khalid. Scientific Reports, Vol. 12, 2022, id. 20053.
- [5] Calado, L. M., M. J. Carmezim, and M. F. Montemor. Rare earth based magnesium alloys – A review on WE series. *Frontiers in Materials*, Vol. 8, January 2022, id. 804906.
- [6] Dutta, S., S. Gupta, and M. Roy. Recent Developments in Magnesium Metal -Matrix Composites for Biomedical Applications: A Review. ACS biomater. *Science & Engineering*, Vol. 6, No. 9, 2020, pp. 4748–4773.
- [7] Casati, R. and M. Vedani. Metal matrix composites reinforced by nano-particles – A review. *Metals*, Vol. 4, 2014, pp. 65–83.
- [8] Sazonov, M. A., T. A. Chernishova, and L. L. Rokhlin. Konstr. I Funkc. Mater, Vol. 2, 2010, pp. 3–22.
- [9] Luo, K., L. Zhang, G. Wu, W. Liu, and W. Ding. Effect of Y and Gd content on the microstructure and mechanical properties of Mg-Y-RE alloys. *Journal of Magnesium and Alloys*, Vol. 7, 2019, pp. 345–354.
- [10] Lianxi, H. and W. Erde. Materials Science and Engineering, Vol. A278, 2000, pp. 267–271.
- [11] Luo, A. Processing, microstructure, and mechanical behavior of cast magnesium metal matrix composites. *Metallurgical and Materials Transactions A: Physical Metallurgy and Materials Science*, Vol. 26A, 1995, pp. 2445–2454.
- [12] Cai, Y., D. Taplin, M. J. Tan, and W. Zhou. Nucleation phenomenon in SiC particulate reinforced magnesium composite. *Scripta Materialia*, Vol. 41, No. 9, 1999, pp. 967–971.

- [13] Saravanan, R. A. and M. K. Surappa. Fabrication and characterisation of pure magnesium-30 vol% SiCP particle composite. *Materials Science and Engineering*, Vol. A276, 2000, pp. 108–116.
- [14] Martin, A. and L. Llorca. Mechanical behaviour and failure mechanisms of a binary Mg 6% Zn alloy reinforced with SiC particulates. *Materials Science and Engineering*, Vol. A201, 1995, pp. 77–87.
- [15] Lee, D. M., B. K. Suh, B. G. Kim, L. S. Lee, and C. H. Lee. Continuous casting process for application of thick aluminium alloy jacet over optical fibre. *Materials Science and Technology*, Vol. 13, 1997, pp. 596–599.
- [16] Ebert, T., F. Moll, and K. V. Kainer. Spray Forming of Magnesium Alloys and Composites. *Powder Metallurgy*, Vol. 40, 1997, pp. 126–130.
- [17] Sankaranarayanan, S., S. Jayalakshmi, and M. Gupta. Materials & Design, Vol. 37, 2012, pp. 274–284.
- [18] Dey, A. and K. M. Pandey. *Reviews on Advanced Materials Science*, Vol. 44, 2016, pp. 168–181.
- [19] Aatthisugan, I., A. R. Rose, and D. S. Jebadurai. Mechanical and wear behaviour of AZ91D magnesium matrix hybrid composite reinforced with boron carbide and graphite. *Journal of Magnesium* and Alloys, Vol. 5, 2017, pp. 20–25.
- [20] Ji-jie, W., G. Jin-hua, and C. Li-qing. TiC/AZ91D composites fabricated by in situ reactive infiltration process and its tensile deformation. *Transactions of Nonferrous Metals Society of China*, Vol. 16, 2006, pp. 892–896.
- [21] Svoboda, M., M. Pahutová, K. Kuchařová, V. Sklenička, and K. U. Kainer. Microstructure and creep behaviour of magnesium hybrid composites. *Materials Science & Engineering, A: Structural Materials: Properties, Microstructure and Processing*, Vol. 462, 2007, pp. 220–224.
- [22] Cho, D. H., J. H. Nam, B. W. Lee, S. O. Yim, and I. M. Park. Thermal expansion properties of carbon nanotube/silicon carbide particlereinforced magnesium composites fabricated by squeeze infiltration. *Metals And Materials International*, Vol. 22, 2016, pp. 332–339.
- [23] Rudajevová, A., J. Balik, and P. Lukáč. Thermal properties of a magnesium hybrid composite: QE22 alloy reinforced with 20 Vol% SiC particles and 5 Vol% Al2O3 fibres. Science and Engineering of Composite Materials, Vol. 9, No. 1, 2000, pp. 11–16.
- [24] Mondal, A. K. and S. Kumar. Dry sliding wear behaviour of magnesium alloy based hybrid composites in transverse direction. *Materials Science Forum*, Vol. 783–786, 2014, pp. 1530–1535.
- [25] Abazari, S., A. Shamsipur, H. Bakhsheshi-Rad, S. Ramakrishna, and F. Berto. Graphene Family Nanomaterial Reinforced Magnesium-Based Matrix Composites for Biomedical Application: A comprehensive review. *Metals*, Vol. 10, 2020, id. 1002.
- [26] Abazari, S., A. Shamsipur, H. R. Bakhsheshi-Rad, and F. Berto. Functionalized carbon nanotube-encapsulated magnesium-based nanocomposites with outstanding mechanical and biological properties as load-bearing bone implants. *Materials & Design*, Vol. 213, 2022, id. 110354.
- [27] Abazari, S., A. Shamsipur, H. R. Bakhsheshi-Rad, and F. Berto. Functionalized carbon nanotube-encapsulated magnesium-based nanocomposites with outstanding mechanical and biological properties as load-bearing bone implants. *Materials & Design*, Vol. 213, 2022, id. 110354.
- [28] Khatkar, S. K. Hybrid magnesium matrix composites: A review of reinforcement philosophies, mechanical and tribological characteristics. *Reviews on Advanced Materials Science*, Vol. 62, 2023, id. 20220294.

- [29] Lianxi, H. and W. Erde. Fabrication and mechanical properties of SiCw/ZK51A magnesium matrix composite by two-step squeeze casting. *Materials Science & Engineering, A: Structural Materials:* Properties, Microstructure and Processing, Vol. 278, 2000, pp. 267–271.
- [30] Jiang, Q. C., X. L. Li, and H. Y. Wang. Fabrication of TiC particulate reinforced magnesium matrix composites. *Scripta Materialia*, Vol. 48, 2003, pp. 713–717.
- [31] Reddy, R. G. and W. Wu. Production of metal/refractory composites by bubbling through a melt, US Patent No. US6, 343, 640, Feb 5, 2002
- [32] Reddy, R. G. A Novel Manufacturing Process for Lightweight Alloy Composites. *Comp Manufact*, Vol. 14, 1998, pp. 5–7.
- [33] Chu, G. and M. K. Premkumar. Mechanism of TiC formation in Al/ TiCin situ metal-matrix composites. *Metallurgical and Materials Transactions A: Physical Metallurgy and Materials Science*, Vol. 24, No. 12, 1993, pp. 2803–2805.
- [34] Wu, W. and R. G. Reddy. In-situ formation of SiC-reinforced Al-Si alloy composites using methane gas mixtures. *Metallurgical and Materials Transactions B: Process Metallurgy and Materials Processing Science*, Vol. 33, 2002, pp. 543–550.
- [35] Zheng, Q., W. Wu, and R. G. Reddy. In-SituProcessing of Al Alloy Composites. *Advanced Engineering Materials*, Vol. 5, No. 3, 2003, pp. 167–172.
- [36] Zheng, Q. and R. G. Reddy. Mechanism of *In-situ* Formation of AlN in Al Melt Using Nitrogen Gas. *Journal of Materials Science*, Vol. 39, No. 1, 2004, pp. 141–149.

- [37] Zheng, Q. and R. G. Reddy. Influence of magnesium on nitridation of molten aluminum from nitrogen bubbling gas. *High Temperature Materials and Processes*, Vol. 22, No. 2, 2003, pp. 63–71.
- [38] Zheng, Q. and R. G. Reddy. Kinetics of In-situ formation of AlN in Al alloy melts by bubbling ammonia gas. Metallurgical and Materials Transactions B: Process Metallurgy and Materials Processing Science, Vol. 34, 2003, pp. 793–804.
- [39] Tyagi, S., Q. Zheng, and R. G. Reddy. "In Situ Synthesis of AlN Reinforced Magnesium Alloy Composites Using Gas Bubbling Method", Aluminum 2004. S. K. Das, editors., TMS, PA, USA, pp. 63–72, 2004.
- [40] HSC Chemistry. Thermodynamic software, Outokumpu Research Oy, Pori, Finland.
- [41] Gokcen, N. A. and R. G. Reddy. *Thermodynamics*, Plenum Publ, New York, USA, 1996.
- [42] Suryanarayana, C. and M. G. Norton. X-ray diffraction A practical approach, 98 Plenum Press, New York, 1998, pp. 227–234.
- [43] Asthana, R., P. K. Rohatgi, and S. N. Tiwari. Microstructure formation during solidification of metal matrix composites. *TMS*, 1993, pp. 11–28.
- [44] Mikucki, B. A., S. O. Shook, W. E. Mercer, and W. G. Green. *Light Metal Age*, Vol. 44, No. 9, 1986, pp. 16–20.
- [45] Scholz, H. and P. Greil. Nitridation reactions of molten Al-(Mg, Si) alloys. *Journal of Materials Science*, Vol. 26, 1991, pp. 669–677.
- [46] Kocherginsky, D. M. and R. G. Reddy. In situ processing of Al/SiC composite. Proceedings In Situ Reactions for Synthesis of Composites, Ceramics, and Intermetallics, TMS, 1995, pp. 159–167.